

1 **Crystal Growth & Design**

2 **In Press, 2020**

3  
4 **Amorphous calcium-magnesium carbonate (ACMC) accelerates**  
5 **dolomitization at room temperature under abiotic conditions**  
6

7 German Montes-Hernandez<sup>a\*</sup>, François Renard<sup>a,b</sup>, Anne-Line Auzende<sup>a</sup>, Nathaniel Findling<sup>a</sup>

8  
9 <sup>a</sup> Univ. Grenoble Alpes, Univ. Savoie Mont Blanc, CNRS, IRD, IFSTTAR, ISTERre, 38000  
10 Grenoble, France

11 <sup>b</sup> The Njord Centre, Department of Geosciences, University of Oslo, box 1048 Blindern, 0316 Oslo,  
12 Norway

13  
14  
15  
16 \*Corresponding author: Dr. German Montes-Hernandez

17 E-mail address: [german.montes-hernandez@univ-grenoble-alpes.fr](mailto:german.montes-hernandez@univ-grenoble-alpes.fr)

18

19           **Abstract**

20   The challenge to produce dolomite  $\text{CaMg}(\text{CO}_3)_2$  at low temperature (20-35°C) over laboratory time  
21   scales remains so far unsuccessful, which has led to long-lasting scientific debates in the last two  
22   centuries. This mineral exerts a major control on the natural carbon dioxide sequestration into  
23   various sedimentary, basaltic and mantellic rocks. The present study reports on specific abiotic  
24   conditions that allows the precipitation of disordered dolomite, high Mg-calcite and high Ca-  
25   magnesite at room temperature over time scales of hours to days. Here we show that an amorphous  
26   calcium magnesium carbonate (ACMC) phase accelerates dolomitization at room temperature.  
27   ACMC is initially precipitated by mixing a carbonate ( $\text{HCO}_3^-/\text{CO}_3^{2-}=1$ ;  $\text{pH}\sim 10.3\sim\text{pK}_{a2}$ ) alkaline  
28   solution with a Mg-Ca ionic solution (Mg molar fraction between 0 and 1). Then, time-resolved in  
29   situ Raman spectroscopy monitored the transformation of ACMC into Mg-rich carbonate minerals.  
30   The initial Mg molar fraction controlled both the reaction mechanism (e.g. nature of transient  
31   crystalline phases) and the kinetics. Nanosized crystallites with short-range order, called disordered  
32   dolomite  $\text{CaMg}(\text{CO}_3)_2$ , precipitated following a complex reaction pathway. Firstly, nesquehonite  
33   ( $\text{MgCO}_3\cdot 3\text{H}_2\text{O}$ : nucleation time = 2.5h), then disordered dolomite ( $\text{CaMg}(\text{CO}_3)_2$ : nucleation time  
34   = 3.2h) and then monohydrocalcite ( $\text{CaCO}_3\cdot\text{H}_2\text{O}$ : nucleation time = 3.4h) formed from ACMC  
35   transformation. Nesquehonite and monohydrocalcite are transient phases that nourish the slow  
36   precipitation of disordered dolomite, which reached a spectral equilibrium after 7 days of reaction.  
37   Direct transformation of ACMC into disordered dolomite was also measured. Our experimental  
38   results demonstrate that disordered dolomite precipitates at room temperature when ideal Mg/Ca  
39   ratio, high-carbonate alkalinity and high ionic-concentration are reached in abiotic systems. This  
40   result suggests the possibility of a physicochemical rather than to biotic control on the formation

41 of disordered dolomite at low temperature in several geosystems.

42

43

44

45

46 **Keywords:** Disordered dolomite, Mg-carbonate, Amorphous carbonate; Time-resolved Raman

47 spectroscopy; Mineral nucleation and growth

## 48 **1. Introduction**

49 Dolomite,  $\text{CaMg}(\text{CO}_3)_2$ , precipitation kinetics and formation mechanism have been widely studied  
50 and controversial claims have been reported in the past two centuries (1). Abiotic precipitation of  
51 dolomite at ambient temperature ( $\sim 25^\circ\text{C}$ ) is virtually impossible within typical laboratory  
52 experimental time scales (2-5). This difficulty is interpreted to originate from the strongly bonded  
53 solvation shells of magnesium ions into aqueous media (2). Dehydration of Mg ions is significantly  
54 facilitated by bacterial activity, including exopolymeric substances, and organic functionalized  
55 surfaces (6-7). Therefore, several studies have claimed that dolomite may precipitate in bio-assisted  
56 systems at ambient laboratory conditions (6-12). Therefore, both textural and crystallographic  
57 characterization, reaction mechanism, and kinetics studies of dolomite precipitation at ambient/low  
58 temperature remain exciting scientific challenges for geochemists and mineralogists (13-17).

59 In addition, the effect of Mg hydration might not be the only factor of inhibition of dolomite  
60 formation at room temperature. Recent studies claimed that a more intrinsic crystallization barrier  
61 and the influence of fluid chemistry (e.g., relative size of the cations in solution) may prevent the  
62 formation of long-range ordered crystallographic structures in dolomite at ambient conditions (3-  
63 5). Lippmann (18) described specific superstructures, called ordering-reflections, in the X-ray  
64 diffraction patterns of dolomite that were related to the regular alternation of monolayers of Ca and  
65 Mg oriented perpendicular to the c-axis of dolomite crystals. This organization indicates an equal  
66 Mg and Ca composition in the structure at the crystal scale. In natural dolomites, structural  
67 imperfections are frequently measured and, sometimes, nanometer sized crystallites with short-  
68 range order may be expected (1). In this last case, the term disordered dolomite (also called  
69 protodolomite) is used because the superstructures ordering reflections, corresponding to the peaks

70 (101), (015) and (021)) in X-ray diffraction patterns, are not detected (13, 19).

71 The present study demonstrates that an amorphous calcium-magnesium carbonate phase (ACMC)  
72 accelerates the dolomitization process at room temperature under abiotic conditions. Herein, an  
73 ACMC phase was instantaneously precipitated by using concentrated ionic solutions ( $\text{HCO}_3^-/\text{CO}_3^{2-}$   
74 solution –  $\text{Mg}^{2+}/\text{Ca}^{2+}$  solution interactions). Then, the persistence time or lifetime (i.e. the duration  
75 until ACMC starts transforming) and transformation of ACMC into new minerals in the interacting  
76 solutions were monitored in real-time by using dynamic Raman spectroscopy (20). We also  
77 investigated the effect of the Mg molar fraction with respect to Ca in solution. This parameter  
78 controls the amount of Mg that can be incorporated into the carbonate crystal lattice and the nature  
79 of transient carbonate phases, allowing to the precipitation of calcite ( $\text{Mg}/(\text{Mg}+\text{Ca}) = 0$ ), low Mg-  
80 calcite ( $\text{Mg}/(\text{Mg}+\text{Ca}) < 10\%$ ), high Mg-calcite ( $10\% < \text{Mg}/(\text{Mg}+\text{Ca}) < 45\%$ ), disordered dolomite  
81 ( $45\% < \text{Mg}/(\text{Mg}+\text{Ca}) \leq 55\%$ ) and high Ca-magnesite ( $\text{Mg}/(\text{Mg}+\text{Ca}) > 60\%$ ), as reported in the  
82 literature (e.g. 21-25).

83 High Mg-calcite and disordered dolomite precipitation at room temperature is frequently related to  
84 bio-mineralization processes, as observed in corals, seashells and many other invertebrates or  
85 observed in laboratory experiments under biotic conditions (16, 21). The present experimental  
86 study demonstrates that disordered dolomite,  $\text{CaMg}(\text{CO}_3)_2$ , can precipitate at low temperature  
87 when ideal Mg/Ca ratio, high-carbonate alkalinity ( $\text{HCO}_3^-/\text{CO}_3^{2-}$  coexistence) and high ionic-  
88 concentration are reached in abiotic or biotic systems. Herein, the formation of an amorphous phase  
89 plays a significant role to produce disordered dolomite

90

## 91 2. Materials and Methods

### 92 2.1. Disordered dolomite $\text{CaMg}(\text{CO}_3)_2$ formation at room temperature

93 The conditions to precipitate disordered dolomite at room temperature (27-31°C) were the  
94 following: 100 mL of  $\text{NaHCO}_3$  (1M) and 100 mL of  $\text{Na}_2\text{CO}_3$  (1M) were placed into a Hastelloy  
95 C22 reactor (Parr, total internal volume of 600 mL) coupled with a Raman probe immersed into  
96 solution/suspension in order to monitor in real-time precipitating carbonate particles and aqueous  
97 carbonate species. This experimental setup was reported previously in Montes-Hernandez group  
98 (20). Raman spectra were collected with a Raman RXN1, Kaiser Optical Systems with an exposure  
99 time of three seconds and averaged over three scans.

100 The carbonate speciation in initial solution was verified by Raman spectroscopy before the  
101 injection of Ca-Mg solution ( $\text{HCO}_3^-$  peaking at  $1016\text{ cm}^{-1}$  and  $\text{CO}_3^{2-}$  peaking at  $1066\text{ cm}^{-1}$ ; see Fig.  
102 S1-A). This carbonate alkaline solution was immediately dispersed by mechanical agitation (400  
103 rpm) before 200 ml of a Ca-Mg solution (Mg molar fraction of 0.75 and Mg concentration of  
104 0.375M) were injected for about 1-2 minutes with a syringe. Following this injection step, the  
105 carbonate speciation and precipitated particles (i.e. transformation of amorphous calcium-  
106 magnesium carbonate APMC into carbonate crystalline phases) were monitored by Raman  
107 spectroscopy for three to seven days, with an acquisition frequency of one Raman spectra every  
108 minute during the first three hours and every five or ten minutes in the remaining time.

109 Selected Raman peaks corresponding to identified mineral phases (see Table S1) were fitted by  
110 using simple or combined Gaussian model in order to estimate both the full wide half maximum  
111 (FWHM) and integrated peak area as a function of time (Movie S1). This calculation provided the

112 peak decomposition necessary to propose relevant reaction mechanisms and to quantify the kinetics  
113 of precipitation of disordered dolomite ( $\text{MgCa}(\text{CO}_3)_2$ ).

## 114 *2.2. Role of Mg molar fraction*

115 The persistence time of amorphous calcium magnesium carbonate (ACMC) and its transformation  
116 into crystalline carbonate phases in the interacting solutions were measured as a function of Mg  
117 molar fraction (Mg molar fraction =  $(V_{\text{Mg}}/(V_{\text{Mg}}+V_{\text{Ca}}))$ ) that was varied between 0 and 1  
118 (experiments 5-11 in Table 1). Herein, the persistence time, also called lifetime, is defined as the  
119 duration over which ACMC is the only precipitate phase present in the suspension before starting  
120 to transform into crystalline carbonate phases. We define the nucleation time of each crystalline  
121 phase as the time where this mineral is detected by Raman spectroscopy. These experiments were  
122 performed following the same protocol described in section 2.1, except for the added volume of  
123 Ca and Mg solutions that was adjusted for each investigated Mg molar fraction. Table 1  
124 summarizes all precipitation experiments performed in this study; each experiment was repeated  
125 at least twice to verify reproducibility of the results.

## 126 *2.3. Ex situ characterization of precipitates*

127 At the end of each experiment, the solid product was recovered by centrifugation and washed twice  
128 with ultrapure water, and once with ethanol. Then, it was dried under a laminar flow of air at 20°C  
129 for 48 h. The dry solid products were stored in plastic flasks for subsequent characterization of  
130 selected samples by Field Emission Gun Scanning Electron Microscopy (FESEM), Transmission  
131 Electron Microscopy (TEM) and powder X-ray diffraction (XRD).

132 Powder XRD spectra were acquired using a Siemens D5000 diffractometer in Bragg-Brentano



133 geometry, equipped with a theta-theta goniometer with a rotating sample holder. Diffraction  
134 patterns were collected using Cu  $k\alpha_1$  ( $\lambda_{k\alpha_1}=1.5406 \text{ \AA}$ ) and Cu  $k\alpha_2$  ( $\lambda_{k\alpha_2}=1.5444 \text{ \AA}$ ) radiations in the  
135 range  $2\theta = 10 - 70^\circ$ , with a step size of  $0.04^\circ$  and a counting time of six seconds per step. For high-  
136 resolution imaging, the solid products were dispersed by ultrasonic treatment in absolute ethanol  
137 for five minutes. Two droplets of the suspension were then deposited directly on an aluminum  
138 support and coated with gold-platinum. The powder was imaged using a Zeiss Ultra 55 FESEM  
139 with a maximum spatial resolution of approximately 1 nm at 15kV. In addition, recovered solid  
140 products from experiments 1 and 2 (Table 1) were shaken in ethanol for a short time in order to  
141 separate the aggregates without any additional treatment. One droplet of the suspension was  
142 deposited on a perforated carbon foil and placed on a conventional copper micro-grid for further  
143 observations with a JEOL 2100F Transmission Electron Microscope (TEM) operating at 200 kV,  
144 equipped with a field emission gun and a high-resolution pole piece achieving a point-to-point  
145 resolution of  $1.8 \text{ \AA}$ . Chemical analyses in selected points on the sample were performed by Electron  
146 Dispersive Spectroscopy (EDS).

147

### 148 **3. Results**

#### 149 *3.1. Precipitation of disordered dolomite at room temperature: Reaction mechanism and kinetics*

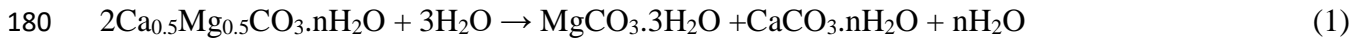
150 Concentrated ionic solutions were chosen to produce an amorphous calcium-magnesium carbonate  
151 (ACMC) phase. Our in-situ Raman spectroscopy data confirmed the instantaneous formation of  
152 ACMC when alkaline carbonate solution ( $\text{HCO}_3^-/\text{CO}_3^{2-}=1$ ) was mixed with Mg-Ca solution (Mg  
153 molar fraction = 0.75), as displayed for three experiments in Fig. S1-B. The precipitated ACMC  
154 ( $\text{Ca}_{0.5}\text{Mg}_{0.5}\text{CO}_3 \cdot n\text{H}_2\text{O}$ ) is characterized by a broad Raman peak at  $1085 \text{ cm}^{-1}$ , shifted  $6 \text{ cm}^{-1}$  away

155 and broader with respect to the peak of amorphous calcium carbonate (ACC:  $\text{CaCO}_3 \cdot n\text{H}_2\text{O}$ ) at 1079  
156  $\text{cm}^{-1}$  (this study), close to the value of  $1080 \text{ cm}^{-1}$  reported in other studies (e.g. 26-27). Time-  
157 resolved Raman spectroscopy shows that ACC starts transforming into crystalline phases after  
158 about 2.5 h of reaction. Nesquehonite ( $\text{MgCO}_3 \cdot 3\text{H}_2\text{O}$ ) is the first detected phase, with a peak at  
159  $1099 \text{ cm}^{-1}$  and a nucleation time of 2.5 h, followed by monohydrocalcite ( $\text{CaCO}_3 \cdot \text{H}_2\text{O}$ ), with a peak  
160 at  $1067 \text{ cm}^{-1}$  and a nucleation time of 3.3 h (Fig. 1). All phases detected in the time-resolved Raman  
161 spectroscopy measurements are summarized in Table S1 and their Raman feature assignment is  
162 supported by previous studies that used systematically ex-situ Raman spectroscopy onto powdered  
163 samples. Nesquehonite and monohydrocalcite are transient phases, i.e. their slow concurrent  
164 dissolution allows the continuous precipitation of disordered dolomite with a Raman peak at  $1094$   
165  $\text{cm}^{-1}$  (Fig. 2). Broad feature of the main peak and low Raman signal in lattice mode at  $300 \text{ cm}^{-1}$   
166 suggest the presence of nanosized crystals, as confirmed by FESEM images that reveal crystallites  
167 with size in the range 20 to 80 nm and forming irregular aggregates (Fig. S2). Herein, we suggest  
168 that this phase is a disordered dolomite, i.e. short-range order forming nanosized crystallites,  
169 because the superstructures ordering reflections ((101), (015) and (021)) are not detected in our  
170 laboratory X-ray powdered diffraction, despite an ideal atomic composition ( $\text{Mg}/\text{Ca}=1$ ) (Fig. S3).  
171 The movie S1 displays the time evolution of the peaks of the main mineral phases during  
172 experiment 2 (Table 1), leading to the formation of disordered dolomite, including the evolution of  
173 ACC, nesquehonite, and monohydrocalcite. The surface areas of the peaks corresponding to  
174 these four phases evolve as a function of time and are used here as proxies to measure the relative  
175 concentrations of these components in the suspension (Fig. S4).

176 From these time-resolved Raman measurements and spectra analyses (Figs. 1, 2 and S4), the  
177 following reactions are proposed, which summarize the mechanism for disordered dolomite  
10

178 formation:

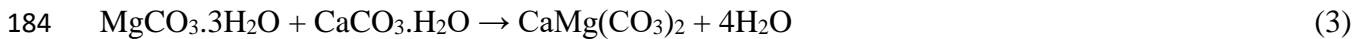
179 **Nesquehonite formation**



181 **Monohydrocalcite formation**

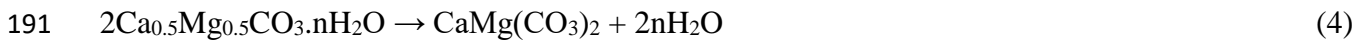


183 **Formation of disordered dolomite via concurrent dissolution of transient phases**



185 Data show that the concurrent slow dissolution of nesquehonite and monohydrocalcite nourish the  
186 precipitation of disordered dolomite. However, disordered dolomite nucleation formed during the  
187 first hours (nucleation time = 3.2h), as detected by fitting the Raman spectra (see Movie S1 and  
188 Fig. S4). These results imply that nesquehonite and monohydrocalcite play a critical retarding  
189 effect on the formation of disordered dolomite as discussed below.

190 The precipitation of disordered dolomite from direct transformation of ACMC could also occur as:



192 This more simple reaction mechanism was detected by time-resolved Raman spectroscopy (Fig. 3,  
193 experiment 1 in Table 1), but with a low experimental reproducibility (once over four total  
194 experiments performed under identical conditions, experiments 1 to 4 in Table 1). In this particular  
195 case, the lifetime of ACMC was larger and equal to 10 hours, as shown on Fig. 3. Herein, the  
196 particle size distribution of disordered dolomite was more homogeneous with an average size of  
197 20 nm (see FESEM images in Fig. S2 for experiment 1). We assumed that, in this particular case,  
198 ACMC reached an ideal Mg/Ca ~ 1 ratio and then its direct transformation into disordered dolomite  
199 could take place, as demonstrated by the Raman data (Fig. 3). However, this chemical event might  
200 be strongly sensitive to small fluctuations of room temperature, fluid chemistry, mechanical  
11

201 agitation and time of mixture of ionic solutions because it happened only once over the four  
202 experiments performed under the same conditions (experiments 1-4 in Table 1).

203 In natural open systems oversaturated with respect to dolomite, fluid chemistry and temperature  
204 fluctuations could inhibit dolomite formation and the precipitated transient phases could remain  
205 persistent and stable for long durations (e.g. 28-29). Such observations may provide an explanation  
206 why dolomite is absent in natural systems presently oversaturated with respect to dolomite.

207

### 208 *3.2. Role of Mg molar fraction*

209 At the investigated carbonate alkaline conditions ( $\text{HCO}_3^-/\text{CO}_3^{2-} = 1$ , 0.5 M for each specie, and  
210  $\text{pH} \sim \text{pK}_{a2} \sim 10.3$ ), both the concentration of Mg and its molar fraction with respect to Ca play a  
211 critical role on the lifetime of ACCM. When the Mg molar fraction is larger than 0.5, the ACCM  
212 lifetime increases substantially (Fig. 4). The reaction mechanism, i.e. the nature of transient  
213 crystalline phases and final recovered products, is also strongly dependent on the concentration of  
214 Mg (see Table 1). For example, when the Mg molar fraction is less or equal than 0.2, vaterite  
215 polymorph is the main transient phase before the formation of low Mg-calcite ( $\text{Mg}_x\text{Ca}_{1-x}\text{CO}_3$  with  
216  $x < 0.1$ ) (Fig. S5). Here, three reaction steps are clearly identified: (1) ACC formation with a lifetime  
217 of 3 minutes; (2) concurrent transformation of ACC into vaterite and Mg-calcite; and (3) slow  
218 transformation of vaterite into low Mg-calcite via coupled dissolution-crystallization process. This  
219 reaction mechanism is in agreement with results obtained from in-situ time-resolved synchrotron-  
220 based wide-angle X-ray scattering (WAXS) and energy dispersive X-ray diffraction (ED-XRD),  
221 despite the difference in pH and Mg concentration (30). At higher Mg molar fraction (e.g. 0.5 and  
222 0.6), high Mg-calcite mesocrystals ( $\text{Mg}_x\text{Ca}_{1-x}\text{CO}_3$  with  $0.1 < x < 0.45$ ) form and the vaterite phase is  
223 not detected (see Table 1). Mg-calcite mesocrystals are micrometric porous aggregates constituted  
12

224 of oriented nano-crystals and that form cauliflower and peanut-like morphologies (Fig. S6). These  
225 peculiar morphologies and the process of aggregation of nanocrystals have been reported in  
226 previous studies (e.g. 22-23). In some studies, high-Mg calcite with peculiar morphologies and  
227 with Mg content into crystal lattice (<45%) was misinterpreted as disordered dolomite (e.g. 15-  
228 16). Therefore, Mg-calcite mesocrystals are not necessarily made of disordered dolomite, except  
229 when the Mg/Ca ratio of the crystal lattice is close to 1.

230 At a Mg molar fraction of 0.75 and under abiotic conditions, we observed the formation of  
231 disordered dolomite ( $\text{CaMg}(\text{CO}_3)_2$ ), as discussed in section 3.1. In complement, X-ray data (Fig.  
232 5) show the (104) reflection in the solid products recovered at the end of experiments that used  
233 different initial Mg molar fraction (see also Table 1. In addition, from Rietveld refinements of XRD  
234 patterns, the Table 2 summarizes the mineral composition and Mg content into calcite crystal  
235 lattice. In general, our results are in agreement with studies that have investigated the influence of  
236 Mg molar fraction on the lifetime of ACC and ACMC phases and their transformation into  
237 crystalline phases (e.g. 28-30). In addition to already published studies, our study reports specific  
238 experimental conditions that allow the synthesis of disordered dolomite by controlling exclusively  
239 the Mg molar content (0.75) and the carbonate alkalinity ( $\text{HCO}_3^-/\text{CO}_3^{2-}=1$ ,  $\text{pH}\sim\text{pK}_{a2}\sim 10.3$ ) at room  
240 temperature (experiments 1-4 in Table 1).

241 Finally, for Mg molar fraction of 0.9 (experiment 10 in Table 1), the lifetime of ACMC was  
242 prolonged to about 4.5 hours and a more complex reaction mechanism was monitored by time-  
243 resolved Raman spectroscopy (Fig. 6). In this experiment, monohydrocalcite ( $\text{CaCO}_3\cdot\text{H}_2\text{O}$ ) was  
244 detected as a transient phase before the formation of disordered dolomite and high Ca-Magnesite  
245 was measured by X-ray diffraction in the product recovered after the experiment (Fig. 5 and Table

246 2). Dypingite ( $\text{Mg}_5(\text{CO}_3)_4(\text{OH})_2 \cdot 5\text{H}_2\text{O}$ ) was also detected, and this hydrated carbonate co-existed  
247 with disordered dolomite and Ca-magnesite until the end of experiment (Fig. 6). These results  
248 demonstrate that the Mg molar fraction controlled the lifetime of ACMC in the interacting  
249 solutions, the reaction mechanism, the kinetics, and the amount of Mg incorporated into the  
250 carbonate.

251

#### 252 **4. Discussion and concluding remarks**

253 Dolomite is a critical mineral that incorporates large volumes of carbon dioxide into a solid form  
254 in many geological environments (1). Primary dolomite formation ( $\text{Mg}^{2+} + \text{Ca}^{2+} + 2\text{CO}_3^{2-}$   
255  $\rightarrow \text{CaMg}(\text{CO}_3)_2$ ) at low temperature (20-35°C) and secondary dolomite formation ( $2\text{CaCO}_3 +$   
256  $\text{Mg}^{2+} \rightarrow \text{CaMg}(\text{CO}_3)_2 + \text{Ca}^{2+}$ ) at higher temperature (diagenetic or hydrothermal, 60-300°C) have  
257 been proposed to explain dolomitization processes in natural environments (1). Primary dolomite  
258 formation has led to controversial claims because ordered dolomite could not be synthesized in  
259 laboratory under abiotic conditions and only disordered dolomite and high Mg-calcite are generally  
260 observed in environments oversaturated with respect to dolomite (2, 15-17). Bio-assisted primary  
261 dolomite formation, and/or formation mediated by living organisms, have been proposed. In such  
262 cases, cellular and intracellular surfaces and exopolymeric substances can overcome the kinetic  
263 barrier to nucleate dolomite (e.g. 6-12). Functionalized organic molecules/surfaces can also  
264 decrease the Mg hydration barrier and catalyze dolomite formation at low temperature (e.g. 31).  
265 However, the reaction mechanism responsible for dolomite formation (e.g., role of transient  
266 amorphous or crystalline phases) and clear proofs or explanations concerning the dolomite  
267 superstructures ordering reflections in the X-ray diffraction patterns have been ambiguously  
268 provided (6, 12). Based on the present study and on recent mechanisms proposed to explain mineral  
14

269 nucleation (e.g. 32-36), we infer that primary dolomite, as initially defined ( $\text{Mg}^{2+} + \text{Ca}^{2+} + 2\text{CO}_3^{2-}$   
270  $\rightarrow \text{CaMg}(\text{CO}_3)_2$ ), has a very low probability to form at room temperature in abiotic or biotic  
271 systems, i.e. through heterogeneous nucleation (pre-existence of reactive surfaces) and a non-  
272 classical nucleation mechanism is therefore expected. The present study demonstrates that transient  
273 amorphous or crystalline phases play a significant role in the formation of disordered dolomite.  
274 Such transient phases can decrease the energy barrier under ideal fluid chemistry conditions (e.g.  
275 direct transformation of ACMC into disordered dolomite), but, they can also retard dolomite  
276 precipitation (e.g. via concurrent dissolution of nesquehonite and monohydrocalcite) as  
277 demonstrated in the present study (Figs. 1, 2, 3 and movie S1). Crystalline phases (e.g. dypingite,  
278 monohydrocalcite, aragonite) can produce an inhibiting effect in laboratory experiments or in some  
279 natural dolomitic environments (1). From the present experimental study, we conclude that ACMC  
280 accelerates dolomitization in a short interval of Mg molar content (0.6-0.75) at low temperature  
281 and the revealed reaction mechanism could exist in natural dolomitic environments such as  
282 lagoons, evaporitic settings, or caves.

283 Another critical point concerning the so-called primary dolomite is the existence of superstructures  
284 ordering reflections in X-ray diffraction patterns (e.g. (101), (015) and (021), Fig. S3). Herein,  
285 some factors can perturb their unambiguous detection. For example, when dolomite crystal size is  
286 larger than 100 nm and coexisting crystalline phases have a low concentration, X-ray powder  
287 diffraction or electron diffraction in TEM allow a clear identification of superstructure ordering  
288 reflections. Conversely, if dolomite crystal size is of the order or smaller than 20 nm (Fig. S7), the  
289 detection of superstructure ordering reflections is more challenging in X-ray diffraction patterns  
290 and by electron diffraction in TEM when nanoparticles are aggregated, despite the ideal Mg content  
291 (Ca/Mg  $\sim$ 1) in the structure lattice (Fig. S3). In such case, disordered dolomite, i.e. short-range

292 ordered crystallographic structures, is assumed and in general, longer range ordering is reached  
293 with an increase of temperature (corresponding to an increase of average size of dolomite crystals)  
294 as already demonstrated in a previous study (13). We claim that the detection limit of laboratory  
295 X-ray diffraction data when nanoparticles exist (the peaks are broader and have lower intensity and  
296 the low intensity of superstructure ordering reflections) and the difficulty to synthesize dolomite in  
297 laboratory experiments have led to contradictory interpretations on the formation of dolomite at  
298 low temperature. In this perspective, the formation of disordered dolomite at low temperature in  
299 abiotic systems can be achieved at room temperature. A future challenge would be to determine  
300 whether a regular alternation of monolayers of Ca and Mg (perpendicular to the c-axis) may exist  
301 in nanosized dolomitic crystals, that would require to develop specific analytical and imaging  
302 methods, such as energy filtered transmission electron microscopy combined with electron energy  
303 loss spectroscopy.

304

305

306

307

308

309

310

311

312

313

314



315 **Acknowledgements**

316           The authors acknowledge funding from the French National Centre for Scientific Research  
317 (CNRS).

318

319

320 **Appendix A. Supplementary data**

321 Supplementary material (1 Table, 7 additional figures and a spectral movie) related to this article can be  
322 found, in the online version, at

323

324

325

326

327

328

329

330

331

332

333

334

335 **References**

- 336 (1) Warren, J. Dolomite: occurrence, evolution and economically important associations. *Earth*  
337 *Sci. Reviews* **2000**, 52, 1-81.
- 338 (2) Deelman, J. C. Breaking Ostwald's rule. *Chemie Der Erde-Geochemistry* **2001**, 61, 224-  
339 235.
- 340 (3) Pimentel, C.; Pina, C. M. The formation of the dolomite-analogue norsethite: Reaction  
341 pathway and cation ordering. *Geochim. Cosmochim. Acta* **2014**, 142, 217-223.
- 342 (4) Hänchen, M.; Prigiobbe, V.; Baciocchi, R.; Mazzotti, M. Precipitation in the Mg-carbonate  
343 system-effects of temperature and CO<sub>2</sub> pressure. *Chem. Eng. Sci.* **2008**, 63, 1012-1028.
- 344 (5) Xu, J.; Yan, C.; Zhang, F.; Konishi, H.; Xu, H.; Teng, H. Testing the cation-hydration effect  
345 on the crystallization of Ca-Mg-CO<sub>3</sub> systems. *Proc. Natl. Acad. Sci.* **2013**, doi:  
346 10.1073/pnas.1307612110.
- 347 (6) Vasconcelos, C.; McKenzie, J. A.; Bernasconi, S.; Grujic, D.; Tien, A. J. Microbial  
348 mediation as a possible mechanism for natural dolomite formation at low temperatures.  
349 *Nature* **1995**, 377, 220-222.
- 350 (7) Warthmann, R.; Van Lith, Y.; Vasconcelos, C.; Mckenzie, J. A.; Karpoff, A. M. Bacterially  
351 induced dolomite precipitation in anoxic culture experiments. *Geology* **2000**, 28, 1091-  
352 1094.
- 353 (8) Sanchez-Roman, M.; McKenzie, J. A.; Wagener, A-de-L. R.; Rivadeneyra, M. A.;  
354 Vasconcelos, C. Presence of sulfate does not inhibit low-temperature dolomite

- 355 precipitation. *Earth Planet. Sci. Lett.* **2009**, 285, 131-139.
- 356 (9) Kenward, P. A.; Goldstein, R. H.; Gonzalez, L. A.; Roberts, J. A. Precipitation of low-  
357 temperature dolomite from anaerobic microbial consortium: the role of methanogenic  
358 Archea. *Geobiology* **2009**, 7, 556-565.
- 359 (10) Deng, S.; Dong, H.; Lv, G.; Jiang, H.; Yu, B.; Bishop, M. E. Microbial dolomite  
360 precipitation using sulfate reducing and halophilic bacteria: Results from Qinghai lake,  
361 Tibetan Plateau, NW China. *Chem. Geol.* **2010**, 278, 151-159.
- 362 (11) Krause, S.; Liebetrau, V.; Gorb, S.; Sanchez-Roman, M.; Mackenzie, J. A.; Treude,  
363 T. Microbial nucleation of Mg-rich dolomite in exopolymeric substances under anoxic  
364 modern seawater salinity: New insight into an old enigma. *Geology* **2012**, 40, 587-590.
- 365 (12) Daye, M.; Higgins, J.; Bosak, T. Formation of ordered dolomite in anaerobic  
366 photosynthetic biofilms. *Geology* **2019**, 47, 510-512.
- 367 (13) Montes-Hernandez, G.; Findling, N.; Renard, F. Dissolution-precipitation reactions  
368 controlling fast formation of dolomite under hydrothermal conditions. *App. Geochem.*  
369 **2016**, 73, 169-177.
- 370 (14) Vandeginste, V.; Snell, O.; Hall, M. R.; Steer, E.; Vandeginste, A. Acceleration of  
371 dolomitization by zinc in saline waters. *Nature Communications* **2019**  
372 doi.org/10.1038/s41467-019-09870-y
- 373 (15) Liu, D.; Xu, Y.; Papineau, D.; Yu, N.; Fan, Q.; Qiu, X.; Wang H. Experimental  
374 evidence for abiotic formation of low-temperature proto-dolomite facilitated by clay

- 375 minerals. *Geochim. Cosmochim. Acta* **2019**, 247, 83-95.
- 376 (16) Huang, Y.-R.; Yao, Q.-Z.; Lia, H.; Wang, F.-P.; Zhou, G.-T.; Fu, S.-Q. Aerobically  
377 incubated bacterial biomass-promoted formation of disordered dolomite and implication  
378 for dolomite formation. *Chem. Geol.* **2019**, 523, 19-30.
- 379 (17) Qiu, X.; Wang, H.; Yao, Y.; Duan, Y. High salinity facilitates dolomite precipitation  
380 mediated by *Haloferax volcanii*DS52. *Earth Planet. Sci. Letters* **2017**, 472, 197-205.
- 381 (18) Lippmann, F., 1973. Sedimentary carbonate minerals. Springer-Verlag, 228pp.
- 382 (19) Montes-Hernandez, G.; Findling, N.; Renard, F.; Auzende, A.-L. Precipitation of  
383 ordered dolomite via simultaneous dissolution of calcite and magnesite : New experimental  
384 insights into an old precipitation enigma, *Cryst. Growth Des.* **2014**, 14, 671-677.
- 385 (20) Montes-Hernandez, G.; Renard, F. Time-resolved in situ Raman spectroscopy of the  
386 nucleation and growth of siderite, magnesite and calcite and their precursors. *Cryst. Growth*  
387 *Des.* **2016**, 16, 7218-7230.
- 388 (21) Long, X.; Ma, Y.; Qi, L. Biogenic and synthetic high magnesium calcite – A review.  
389 *J. Struc. Bio.* **2014**, 185, 1-14.
- 390 (22) Yu, P. T.; Tsao, C.; Wang, C. C.; Chang, C. Y.; Chan, C. C. High-Magnesium  
391 Calcite Mesocrystals: Formation in Aqueous Solution under Ambient Conditions.  
392 *Angewandte Chemie Int.* **2017**. 51, 16420-16424, doi.org/10.1002/anie.201708507.
- 393 (23) Landers, J. J. M.; Dey, A.; Bomans, P. H. H.; Spielmann, J.; Hendrix, M. M. R. M.;  
394 de With, G.; Meldrum, F. C.; Harder, S.; Sommerdijk N. A. J. M. High-Magnesian Calcite

- 395 Mesocrystals: A Coordination Chemistry Approach. *J. Am. Chem. Soc.* **2012**, 134, 1367-  
396 1373.
- 397 (24) Yang, H.; Chai, S.; Zhang, Y.; Ma, Y. A study on the influence of sodium carbonate  
398 concentration on the synthesis of high Mg calcites. *CrystEngComm* **2016**, 18, 157-163.
- 399 (25) Romaneck, C.; Jimenez-Lopez, C.; Rodriguez-Navarro, A.; Sanchez-Roman, M.;  
400 Sahai N.; Coleman, M. Inorganic synthesis of Fe–Ca–Mg carbonates at low temperature.  
401 *Geochim. Cosmochim. Acta* **2009**, 73, 5361-5376.
- 402 (26) Wehrmeister, U.; Jacob, D. E.; Soldati, A. L.; Loges, N.; Hager, T.; Hofmeister W.  
403 Amorphous, nanocrystalline and crystalline calcium carbonates in biological materials. *J.*  
404 *Raman Spectrosc.* **2010**, 5, 926-935, doi.org/10.1002/jrs.2835.
- 405 (27) Wang, D.; Hamm, L. M.; Bodnar, R. J.; Dove, P. M. Raman spectroscopic  
406 characterization of the magnesium content in amorphous calcium carbonates. *J. Raman*  
407 *Spectrosc.* **2012**, 43, 543-548.
- 408 (28) Rodriguez-Blanco, J. D.; Shaw, S. Bots, P.; Roncal-Herrero, T.; Benning, L. G. The  
409 role of Mg in the crystallization of monohydrocalcite. *Geochim. Cosmochim. Acta* **2014**,  
410 127, 204-220.
- 411 (29) Rodriguez-Blanco, J. D.; Shaw, Benning, L. G. A route for the direct crystallization  
412 of dolomite. *Amer. Miner.* **2015**, 100, 1172-1181.
- 413 (30) Rodriguez-Blanco, J. D.; Shaw, S.; Bots, P.; Roncal-Herrero, T.; Benning, L. G. The  
414 role of pH and Mg on the stability and crystallization of amorphous calcium carbonate. *J.*

- 415 *Alloys Compd.* **2012**, 536S, S477– S479.
- 416 (31) Roberts, J. A.; Kenward, P. A.; Fowle, D. A.; Golstein, R. H.; Gonzalez, L. R.;  
417 Moore, D. S. Surface chemistry allows for abiotic precipitation of dolomite at low  
418 temperature. *Proc. Natl. Acad. Sci.* **2013**, 110(36), 14540–14545
- 419 (32) Gebauer, D.; Völkel, A.; Cölfen, H. Stable prenucleation calcium carbonate  
420 clusters. *Science* **2008**, 322, 1819-1822.
- 421 (33) Dideriksen, K.; Frandsen, C.; Bovet, N.; Wallace, A. F.; Sel, O.; Arbour, T.;  
422 Navrotsky, A.; De Yoreo, J. J.; Banfield, J. F. Formation and transformation of a short range  
423 ordered iron carbonate precursor. *Geochim. Cosmochim. Acta*, **2015**, 164, 94–109.
- 424 (34) Gower, L. B.; Tirrell, D. A. Calcium carbonate films and helices grown in solution of  
425 poly (aspartate). *J. Cryst. Growth*, **1998**, 191, 153-160.
- 426 (35) Gebauer, D.; Kellermeier, M.; Gale, J. D.; Bergstrom, L.; Colfen, H. Pre-nucleation  
427 clusters as solute precursors in crystallization. *Chem. Soc. Rev.*, **2014**, 43, 2348-2371.
- 428 (36) Wang, T.; Cölfen, H.; Antonietti, M. Nonclassical crystallization: Mesocrystals and  
429 morphology change of CaCO<sub>3</sub> crystals in the presence of a polyelectrolyte additive. *J. Am.*  
430 *Chem. Soc.* **2005**, 127, 3246-3247.

431 Table 1. List of experiments with time-lapse Raman spectroscopy for precipitation of disordered  
 432 dolomite at room temperature and influence of Mg molar ratio. A constant carbonate alkalinity of  
 433  $\text{HCO}_3^-/\text{CO}_3^{2-}=1$  (0.5M) and a total cationic (Mg-Ca) concentration of 0.5M were imposed.

Exp.	Temperature (°C)	Mg molar fraction	Exp. duration (days)	Lifetime of APMC (min. / h)	Mineral transient phase(s)	Final mineral phase(s)
1	27	0.75	3	10 h	none	disordered dolomite*
2	31	0.75	7	2.5 h	nesquehonite monohydrocalcite	disordered dolomite*
3	31	0.75	7	2.3 h	nesquehonite monohydrocalcite	disordered dolomite
4	30	0.75	10	1.9 h	nesquehonite monohydrocalcite	disordered dolomite
5	28	0	1	0.75 min.	vaterite	calcite*
6	28	0.05	1	1.75 min.	vaterite	calcite*
7	29	0.20	2	3 min.	vaterite	low Mg-calcite*
8	27	0.5	2	3 min.	none	high Mg-calcite*
9	28	0.6	2	30 min.	none	high Mg-Calcite*
10	29	0.9	2	4.5 h	monohydrocalcite	disordered dolomite* dypingite*
11	28	1	3	2 h	none	Dypingite

434 \* these phases were also characterized by powder X-ray diffraction

435 Table 2. Mineral carbonate composition and Mg content in lattice structure identified from Rietveld  
 436 refinement of X-ray diffraction patterns. In experiment 10, aragonite, dypingite and eteilite were  
 437 also detected.

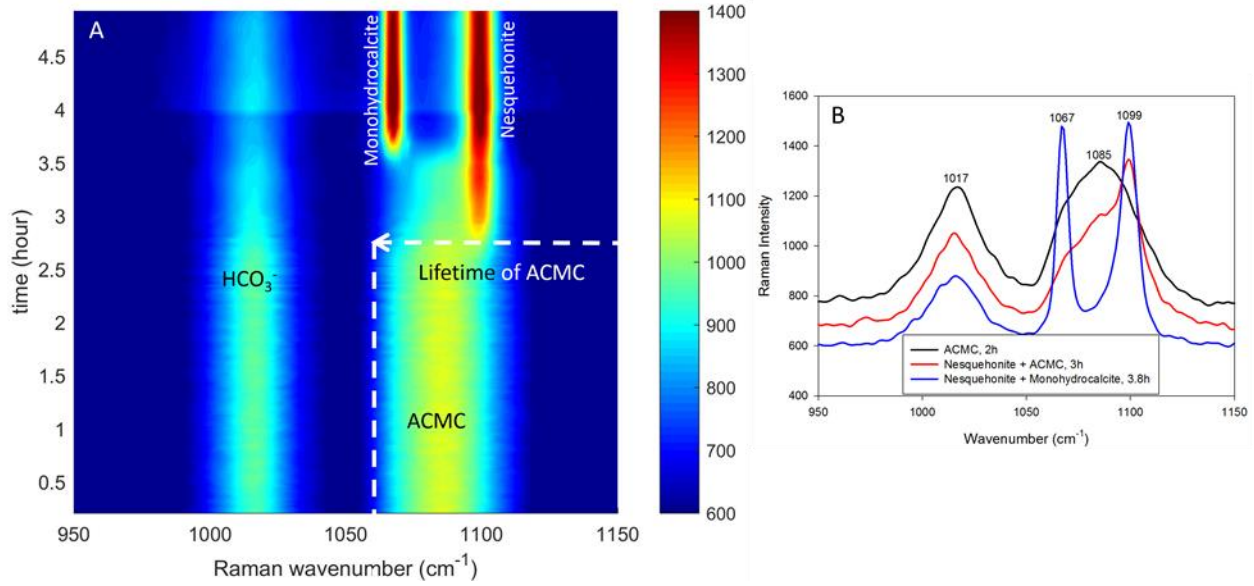
Exp.	Mg molar fraction	Calcite	Low Mg- Calcite	High Mg- Calcite	Disordered Dolomite	High Ca- Magnesite
5	0	CaCO <sub>3</sub>	none	none	none	None
6	0.05	CaCO <sub>3</sub>	none	none	none	none
7	0.20	CaCO <sub>3</sub>	Mg <sub>0.05</sub> Ca <sub>0.95</sub> CO <sub>3</sub>	none	none	none
8	0.50	none	none	Mg <sub>0.15</sub> Ca <sub>0.85</sub> CO <sub>3</sub> Mg <sub>0.23</sub> Ca <sub>0.77</sub> CO <sub>3</sub>	none	none
9	0.6	none	none	Mg <sub>0.35</sub> Ca <sub>0.65</sub> CO <sub>3</sub>	none	none
1	0.75	none	none	none	Mg <sub>0.49</sub> Ca <sub>0.51</sub> CO <sub>3</sub>	none
10	0.9 <sup>x</sup>	none	Mg <sub>0.07</sub> Ca <sub>0.93</sub> CO <sub>3</sub>	none	Mg <sub>0.45</sub> Ca <sub>0.55</sub> CO <sub>3</sub>	Mg <sub>0.68</sub> Ca <sub>0.32</sub> CO <sub>3</sub>

438

439



440



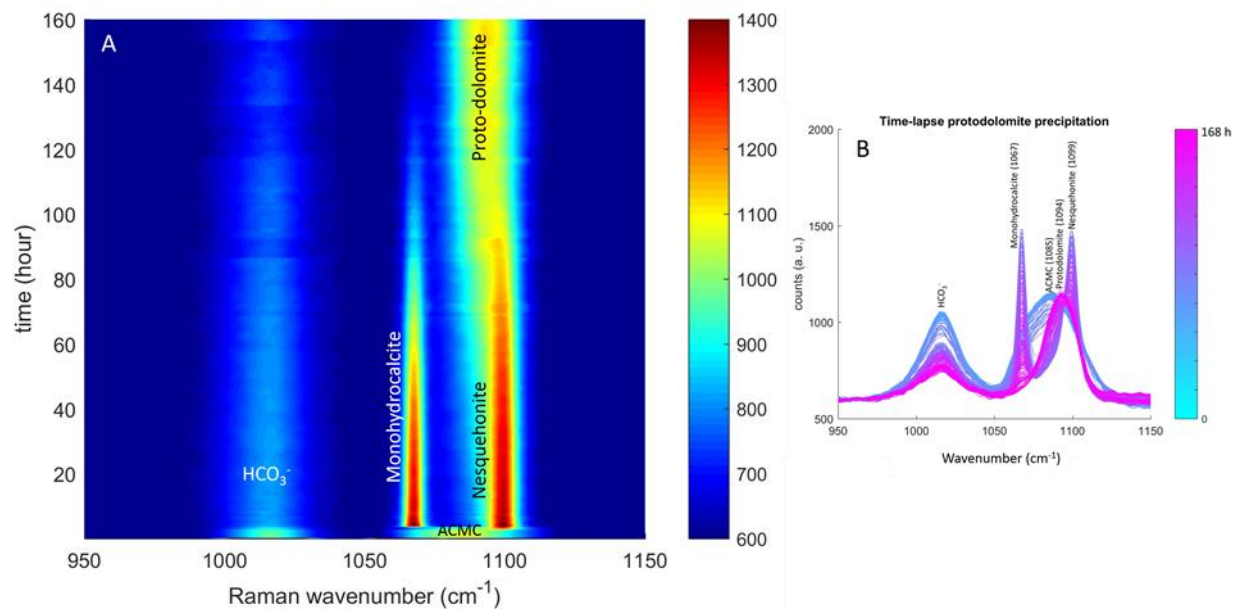
441

442

443

444

445 Figure 1. Time-lapse Raman spectroscopy monitoring of amorphous calcium-magnesium  
446 carbonate (ACMC) transformation into crystalline phases during the first four hours of experiment  
447 2 (Table 1). The lifetime of ACMC and positions of crystalline phases are indicated.



448

449

450

451

452

453

454

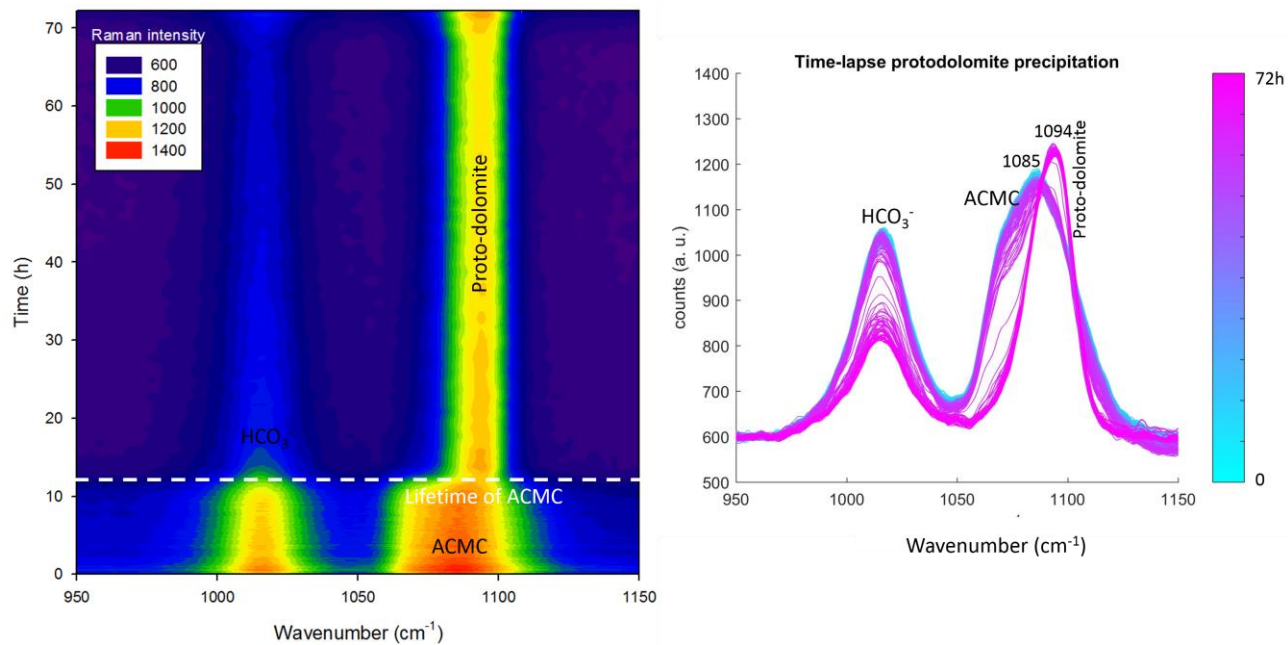
Figure 2. Time-lapse Raman spectroscopy monitoring of the formation of disordered dolomite from

455

ACMC in experiment 2 (Table 1). Left: evolution of the two transient phases, nesquehonite and

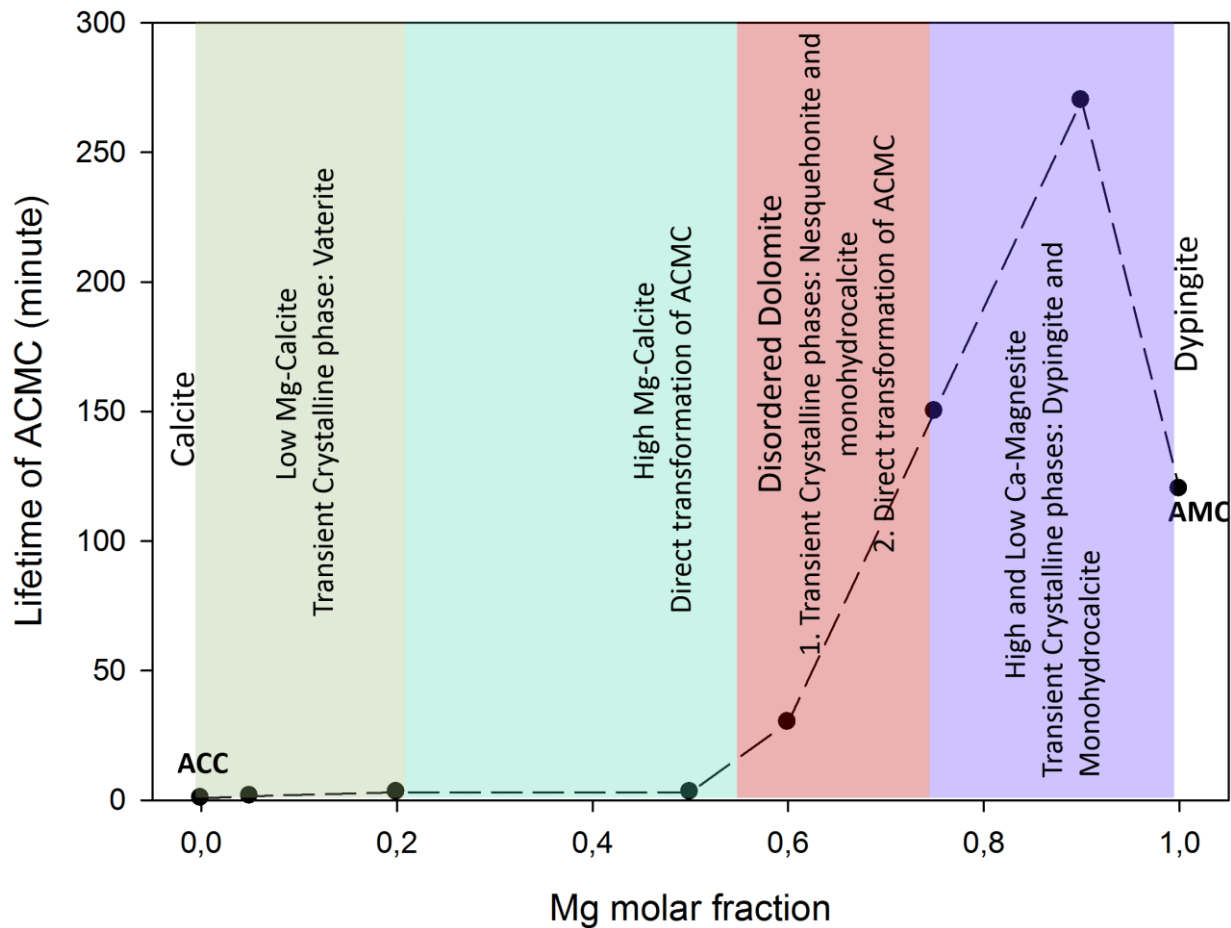
456

monohydrocalcite. Right: time-lapse evolution of the main peaks.



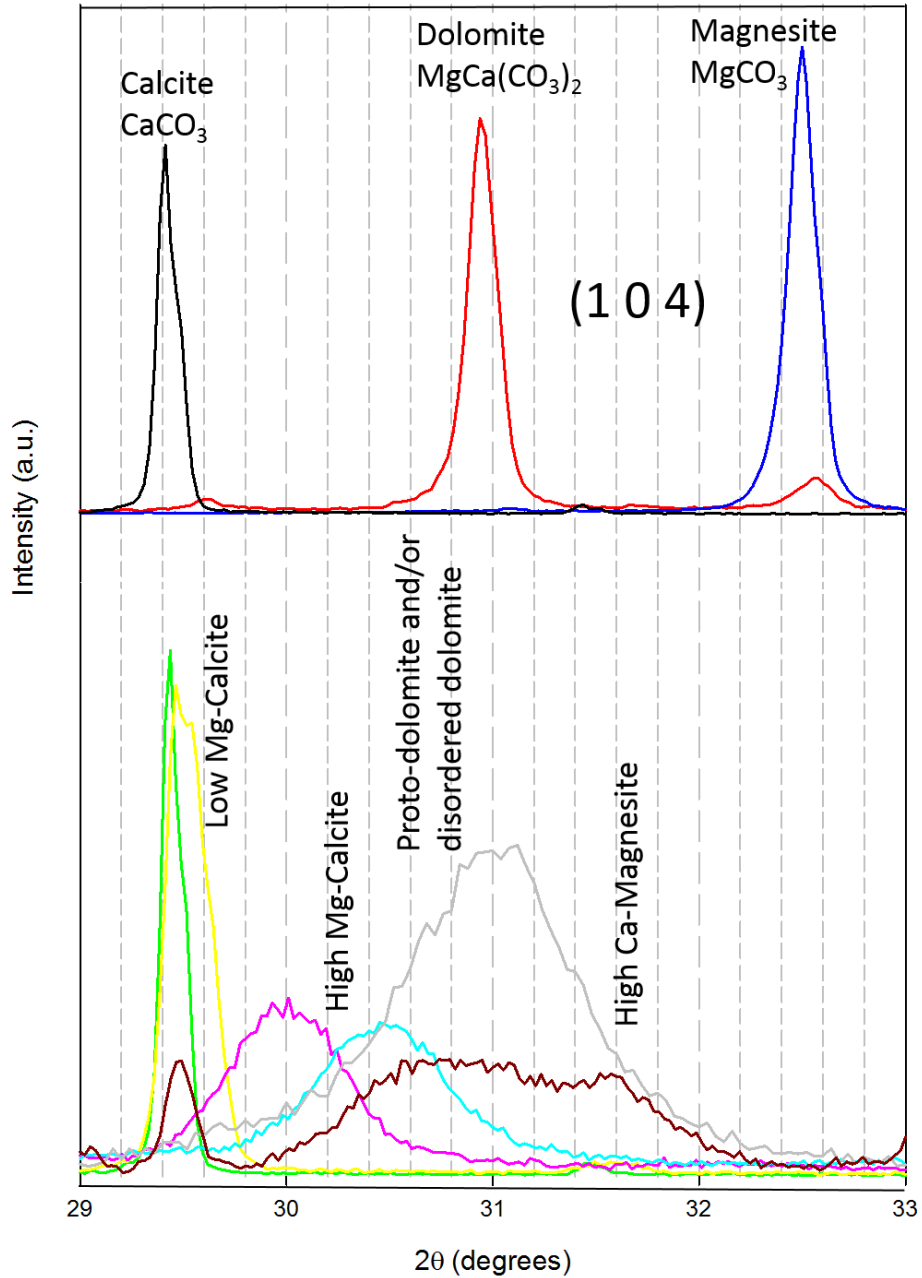
457

458 Figure 3. Left: Time-lapse Raman spectroscopy monitoring of the formation of disordered dolomite  
 459 from direct transformation of ACMC in experiment 1 (Table 1). Right: time-lapse evolution of the  
 460 main peaks.



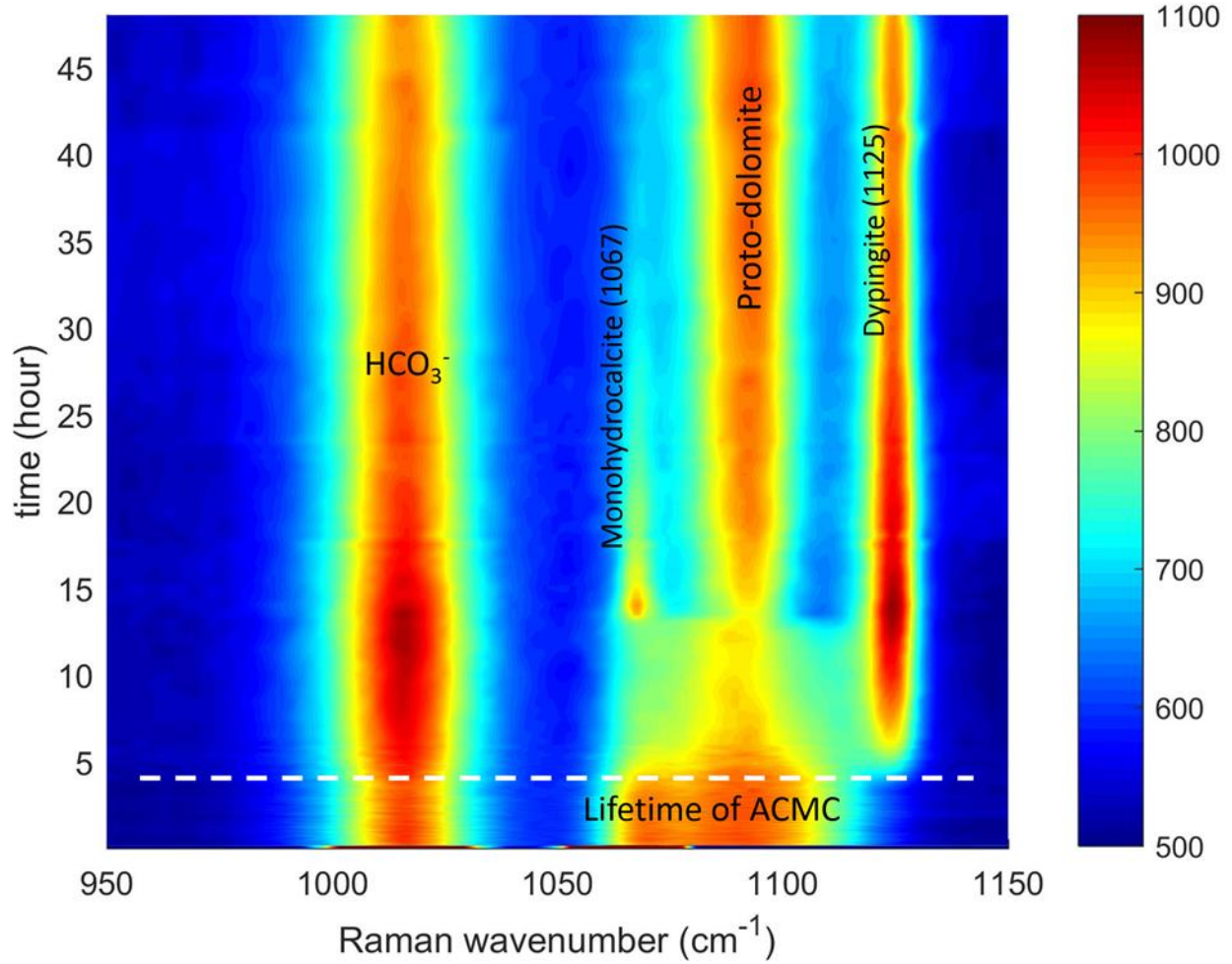
461

462 Figure 4. Lifetime of ACMC determined from time-resolved Raman measurements as a function  
 463 of Mg molar fraction. Eight precipitation experiments were performed with initial alkaline solution  
 464 ( $\text{HCO}_3^-/\text{CO}_3^{2-}$  molar ratio =1, and 0.5 M) at room temperature. ACC: amorphous calcium  
 465 carbonate; ACCM: amorphous calcium-magnesium carbonate; AMC: amorphous magnesium  
 466 carbonate.



467

468 Figure 5. X-ray diffraction data showing the (104) reflection for calcite, dolomite and magnesite  
 469 references (13) and solids obtained for different initial Mg molar fraction in the solution: 0.05:  
 470 green; 0.2: yellow; 0.5: pink; 0.6: cyan; 0.75: gray; 0.9: dark red, corresponding to experiments 6-  
 471 10 in Table 1, respectively.



472  
 473 Figure 6. Time-lapse Raman spectroscopy monitoring of the formation of disordered dolomite from  
 474 ACMC in experiment 10 (Table 1). Monohydrocalcite is a transient phase (Mg molar fraction of  
 475 0.9) and dypingite (hydrated Mg carbonate mineral:  $\text{Mg}_5(\text{CO}_3)_4(\text{OH})_{2.5}\text{H}_2\text{O}$ ) coexist with  
 476 disordered dolomite until the end of experiment.

477

478

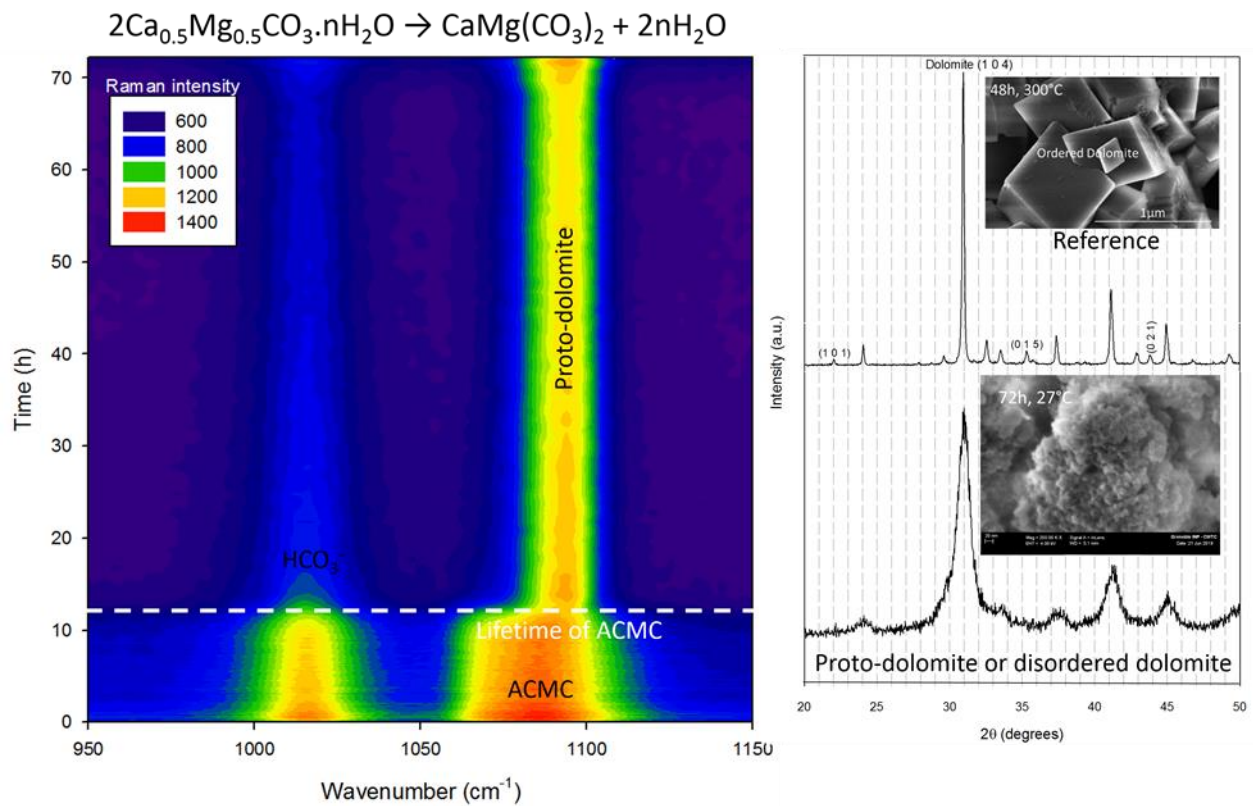
479

480 **Amorphous calcium-magnesium carbonate (ACMC) accelerates dolomitization at room**  
481 **temperature under abiotic conditions**

482 By German Montes-Hernandez, François Renard, Anne-Line Auzende, Nathaniel Findling

483

484 **Table of Contents Graphic**



486 **Synopsis:** The present study reports on specific abiotic conditions that allows the precipitation of  
487 disordered dolomite, high Mg-calcite and high Ca-magnesite at room temperature over time scales  
488 of hours to days. Here we show that an amorphous calcium magnesium carbonate (ACMC) phase  
489 accelerates dolomitization at room temperature.